Available online at www.sciencedirect.com
SCIENCE DIRECT
Journal of Power Sources 156 (2006) 615–619
JOURNAL OF POWER SOURCES
www.elsevier.com/locate/jpowsour

Short communication

Exfoliation-induced nanoribbon formation of poly(3,4-ethylene dioxythiophene) PEDOT between MoS_2 layers as cathode material for lithium batteries

A. Vadivel Murugan [a,*], Mathieu Quintin [b], Marie-Helene Delville [b], Guy Campet [b], Chinnakonda S. Gopinath [c], K. Vijayamohanan [c,**]

[a] *Centre for Materials for Electronics Technology (C-MET), Department of Information Technology, Government of India, Off-Pashan Road, Panchawati, Pune 411008, India*
[b] *Institut de Chimie de la Matière Condensée de Bordeaux (ICMCB), CNRS, 87 Avenue du Dr. A Schweitzer, 33608 Pessac, France*
[c] *National Chemical Laboratory, Dr. Homi Bhabha Road, Pune 411008, India*

Received 14 March 2005; accepted 7 June 2005
Available online 6 September 2005

Abstract

A new type of layered nanocomposite synthesized by delaminated MoS_2 nanosheets and poly(3,4-ethylenedioxythiophene) (PEDOT) are restacked to produce alternate polymer nanoribbons between layers of MoS_2 with an interlayer distance of ~1.38 nm. The unique properties of resulting nanocomposite are investigated by powder XRD, XPS, SEM, TEM, and four-probe conductivity measurements. The obtained nanocomposite can be used as a cathode material for a small power rechargeable lithium battery as demonstrated by the electrochemical insertion of lithium into the PEDOT/MoS_2 nanocomposite. A significant enhancement in the discharge capacity (100 mAh g^{-1}) is observed compared with that (40 mAh g^{-1}) for MoS_2.

Keywords: Organic–inorganic nanocomposite; PEDOT-nanoribbons; MoS_2; Cathode material; Lithium batteries

1. Introduction

Low-dimensional materials have attracted much attention recently due to their novel physicochemical properties in comparison with bulk materials. For example, zero-dimensional nanoparticles and one-dimensional nanostructures, such as nanotubes, nanowires, and nanorods, have been investigated intensively both for their size and shape-dependent fundamental properties and also for their potential applications [1–3]. Low dimensional systems comprising a variety of two-dimensional lamellar nanocomposites have also been synthesized by chemically delaminating a layered host into molecular single layers [4,5]. One approach to modify the properties of layered inorganic oxides, sulfides and graphite is through the intercalation of guests into this host using suitable procedures [6–10]. For example, many transition metal dichalcogenides have lamellar structures that are amenable to intercalation, and such modified materials also have interesting applications [11]. In particular, MoS_2 has drawn great attention due to its several important applications as an inorganic host for polymers, for battery cathodes [12], and an encapsulating support for magnetic materials [13]. In the continuing quest for preparing hybrid materials with novel or enhanced properties, insertion of conducting polymers into layered host materials and other structurally organized environments is a topic of considerable interest because

* Corresponding author. Tel.: +91 20 25898390; fax: +91 20 25898180.
** Corresponding author.
E-mail addresses: vadivel12@hotmail.com (A.V. Murugan), viji@ems.res.ncl.in (K. Vijayamohanan).

0378-7753/$ – see front matter © 2005 Elsevier B.V. All rights reserved.
doi:10.1016/j.jpowsour.2005.06.022

the resulting organic–inorganic nanostructures can possess novel electrical, structural, and mechanical properties. Such systems can potentially show hybrid properties that are synergistically derived from both the host and the guest [12].

Recently, we have demonstrated the synthesis of a conducting poly(3,4-ethylene dioxythiophene) based nanocomposite and its application as an electrode material for electrochemical power sources [10,16]. Poly(3,4-ethylenedioxythiophene) (PEDOT), one of the recently found excellent conducting polymers, has been reported to exhibit greatly enhanced stability compared with other conducting polymers [14,15]. Indeed, it appears to be one of the most stable conducting polymers presently available [16] and has been attracting growing interest for applications in supercapacitors and electrochromic devices [17,18]. Here, we focus on the synthesis and characterization of an organo–inorganic PEDOT/MoS_2 nanocomposite, where PEDOT forms nanosheets in the interlayer spacing. The primary objective is to understand the specific molecular interactions between PEDOT and MoS_2 using various spectroscopic and electrochemical techniques to demonstrate how these interactions enhance the properties of the PEDOT/MoS_2 nanocomposite. These observations are supported by several physicochemical data including the microstructure of the PEDOT/MoS_2 nanocomposite, after the formation of the polymer nanoribbons between the MoS_2 layers. To our knowledge, this is the first study of the preparation of a PEDOT/MoS_2 nanocomposite as well as the demonstration that it is possible to increase the specific capacity for potential applications of the nanocomposite in low-power, rechargeable lithium batteries.

2. Experimental

The delamination of a MoS_2 nanosheet was produced by the suspension of 0.08 g mL^{-1} of Li_xMoS_2 in water followed by sonication. To this suspension, 4.6 mM of 3,4-ethylenedioxy thiophene (EDOT) monomer was added drop-wise and was refluxed with a single layer suspension of exfoliated MoS_2 to ensure complete mixing. To this mixture, 8.5 g of the oxidizing agent, iron (III) chloride dissolved in double-distilled water was added drop-wise. After acidification to pH 2, the suspension was reflocculated under refluxed conditions for 10 h. The degree of intercalation was found to vary with the length of refluxing time following acidification. The resulting PEDOT/MoS_2 solid was filtered off and washed repeatedly with water and ethanol. The dark bluish-black powder was dried in air.

The synthesized product was characterized and analyzed by X-ray diffraction (Rigaku miniflex) equipped with Ni-filtered Cu Kα (1.542 Å) radiation and a graphite crystal monochromator. X-ray photoemission spectra (XPS) were recorded with a VG Microtech Multilab ESCA 3000 spectrometer using a non-monochromatized Al Kα X-ray source ($h\nu$ = 1486.6 eV). The base pressure in the chamber was maintained in the range of 10^{-10} Torr. The energy resolution of the spectrometer was set at 1.0 eV with Al Kα radiation at a pass energy of 50 eV. Binding energy (BE) calibration was performed with the Au $4f_{7/2}$ core level at 83.9 eV. The BE of carbon (284.9 eV) was used as a reference. The error in all the BE values reported here is within ±0.1 eV. Electronic conductivity measurements were carried out on compacted pellets by using the four-probe conductivity method. Scanning electron microscopy (SEM Philips XL-30) and transmission electron microscopy (TEM, JEM-2010, JEOL) were performed on the powdered samples. For electrochemical studies, electrodes were prepared by mixing the PEDOT/MoS_2 powder or pristine MoS_2 with carbon black and a PTFE binder (70:25:5, w/w), followed by compaction into pellets and drying under a primary vacuum for 3 h at 80 °C. Each composite cathode was coupled with a lithium foil anode in 1 M $LiClO_4$ dissolved in a mixture of ethylene carbonate and dimethyl carbonate (EC:DMC = 1:1) to form the electrochemical cell. All charge–discharge measurements were performed in a galvanostatic mode using a computer-controlled potentiostat/galvanostat. All manipulations of air-sensitive materials, as well as cell assemblies, were carried out in an argon-filled glove box.

3. Results and discussion

The encapsulation of polymers between the interlayer van der Waals' gap of the MoS_2 is demonstrated by X-ray powder diffraction, which shows in Fig. 1(a) and (b) of the typical XRD pattern of pristine 2H-MoS_2 and poly(3,4-ethylenedioxythiophene) PEDOT/MoS_2 nanocomposite, for which rather sharp and intense (0 0 1) reflections are observed with shifts to lower angles that indicates an increase in interlayer spacing. The latter pattern exhibits a characteristic saw-tooth shape composed of asymmetrically broadened peaks.

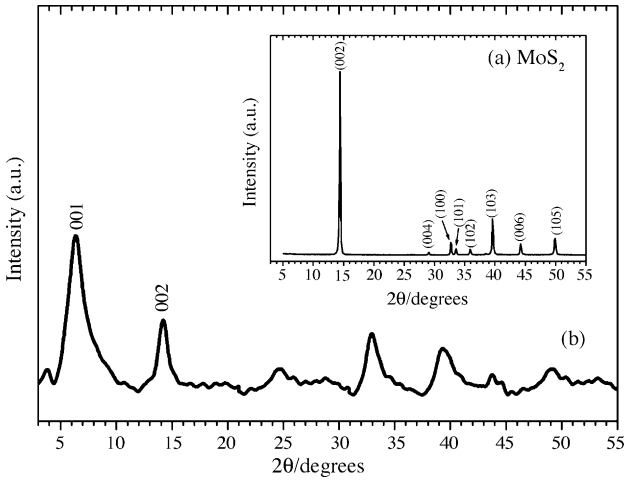

Fig. 1. Comparative powder X-ray diffraction patterns of: (a) 2H-MoS_2 powder; (b) PEDOT/MoS_2 nanocomposite.

This is a consequence of the Warren effect [19] which arises from the fact that for a two-dimensional layer, the reciprocal lattice becomes a line perpendicular to the layer and so, for higher diffraction angles, a continuous distribution of diffraction intensity appears. The pattern in Fig. 1(a), displays all the $h\,k\,l$ values for 2H-MoS_2, but the pattern in Fig. 1(b) shows only 0 0 1 and 0 0 2 peaks. In Li_xMoS_2 and all other MoS_2-based intercalation compounds as well as molybdenum, clustering in the a–a plane induces superstructure lines. This well-known behaviour also occurs in the PEDOT/MoS_2 intercalation compound. It is related to some electron transfer from the guest (polymer) species to MoS_2 host. Thus, an increase in the interlayer spacing (13.76 Å) of PEDOT/MoS_2, indicates substantial incorporation of the conducting polymer between the layers. This change in the interlayer distance is consistent with the intercalated PEDOT chains being oriented with the planes of the thiophene rings perpendicular to the layers. Therefore, hydrogen bonds and also π-electrons between the organic and inorganic components are expected. It is likely that these materials constitute a new PEDOT/MoS_2 composite phase which consists of a monolayer of PEDOT chains intercalated within the MoS_2 layers. Such structures have also been reported for other organic molecules [19] and conducting polymers [10,20] intercalated in transition metal sulfide/oxide hosts.

PEDOT and PEDOT/MoS_2 composite materials were subjected to XPS analysis and the results from molybdenum 3d and sulfur 2p core levels of the above samples are shown in Fig. 2(a) and (b), respectively. Composite material was made into pellets and the surface was scraped in situ in the XPS chamber to remove any degradation/air oxidation product. Interestingly, the PEDOT/MoS_2 surface analyzed prior to scraping (dotted line in Fig. 2(a)) shows a large amount of MoO_x in addition to carbonates and hydroxides. This can be attributed to contamination of the surface by air, which can be completely removed by scraping. The Mo 3d core level spectrum shows spin-orbit doublet peaks at 229.1 and 232.3 eV for the PEDOT/MoS_2 composite (bold line) after scraping. This is typical for MoS_2 sulfide [21]. This procedure ensures that the surface analyzed after scraping offers an uncontaminated representative of PEDOT/MoS_2 and the atmospheric degradation is limited to only the top surface. The S 2p core level from PEDOT displays a peak at 164 eV that is typical for thiophene sulfur [21]. The main S 2p peak at 162 eV for PEDOT/MoS_2 after scraping is due to S from MoS_2. The S 2p core level from PEDOT/MoS_2 also shows a shoulder around 163 eV and this suggests with intercalation of the PEDOT, there is some charge transfer from Mo to thiophene units, in addition to the probably strong van der Waals' interaction.

Scanning electron micrographs of the MoS_2 and the PEDOT/MoS_2 composite are presented in Fig. 3(a) and (b), respectively. PEDOT/MoS_2 has, as expected, a clearly distinctive morphology. It is therefore evident that the incorporation of PEDOT into the MoS_2 is accompanied by morphological changes. The micrographs also suggest that

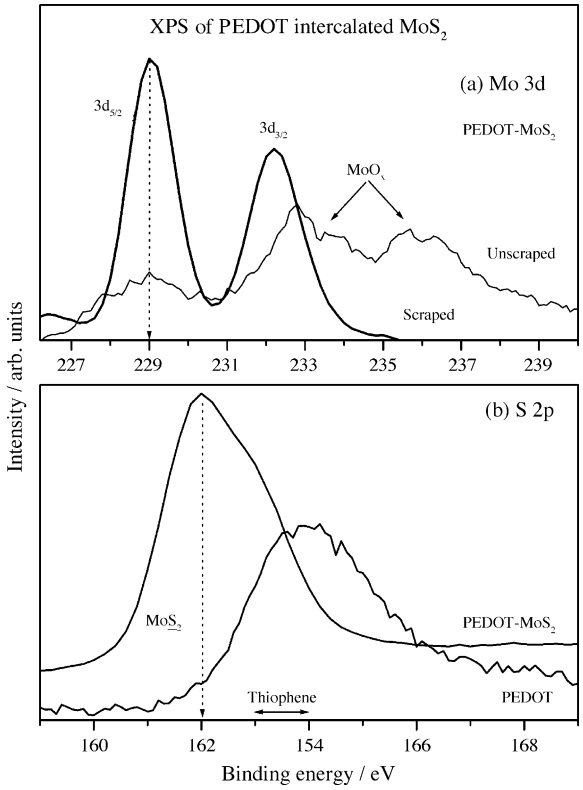

Fig. 2. XPS of (a) Mo 3d core level and (b) S 2p core level from PEDOT and PEDOT intercalated MoS_2; unscraped PEDOT–MoS_2 surface shows MoO_x species due to atmospheric oxidation although physical scraping removes the contamination.

there is no bulk deposition of polymer on the surface of the micro-crystallites. A transmission electron microscopy (TEM) image of MoS_2 shows thick particles with a few micrometer dimensions (Fig. 3(c)), whereas the morphology of the nanoribbons of the PEDOT/MoS_2 nanocomposite, see Fig. 3(d), are in agreement with the results of XRD patterns. As can be seen from the TEM image, low scattering power causes bright contrast for white lines of conducting polymer nanoribbons between dark fringes of MoS_2 host layers (Fig. 3(d)). Interestingly, the stacking length in the c-direction is apparently shorter compared with that in both the a and the b directions for the hybrids (Fig. 3(d)); this would be considered as an enhancement of 'bidimensionality'. The interlayer spacing of PEDOT/MoS_2 has been estimated by measuring the length from one dark line to the nearest one; it gives ∼14 Å, a value which is in good agreement with the above reported XRD results (13.76 Å).

The electron transport behaviour of MoS_2 is expected to be modified significantly by the intercalation of PEDOT as the carrier density can undergo a dramatic change. The four-probe dc electronic conductivity of the PEDOT/MoS_2 nanocomposite measured at different temperatures shows a linear increase in conductivity that is indicative of thermally activated electron transport behaviour as shown in Fig. 4. Similar behaviour for other nanocomposites has

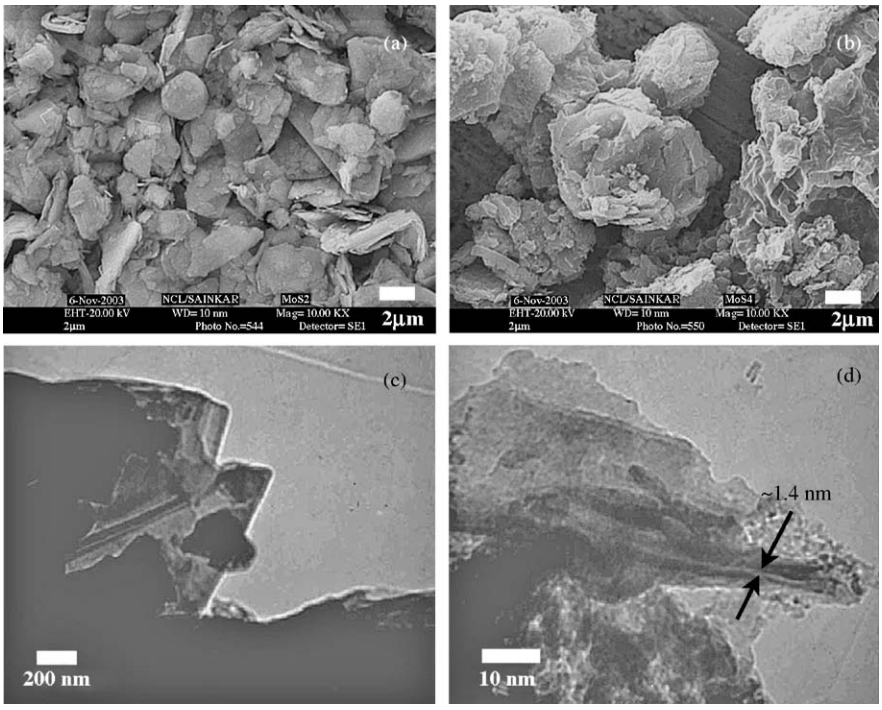

Fig. 3. Scanning electron micrographs of (a) MoS_2 and (b) PEDOT/MoS_2; transmission electron images of (c) MoS_2 (d) PEDOT nanoribbons intercalated into MoS_2 layers morphology of nanocomposite.

recently been reported [16]. The room-temperature conductivity of pristine MoS_2 and the PEDOT/MoS_2 composite are 1.09×10^{-2} and 2.09×10^{-1} S cm^{-1}, respectively. The conductivity of PEDOT/MoS_2 is therefore almost one order more than that of pristine MoS_2. This increase in conductivity is, however, less than that observed for PEDOT/V_2O_5 hybrids for which there was a three orders of magnitude increase in conductivity compared with that of the pristine oxide [10,16].

Potential versus capacity curves are shown in Fig. 5(a) for a typical (third) discharge carried out for MoS_2 and the PEDOT/MoS_2 hybrid at a constant current density of 15 mA cm^{-2} over the voltage range 4.4–1 V (versus Li^+/Li), which corresponds to an uptake of ~1.5 lithium per MoS_2 unit. Also, the open-circuit voltage (OCV) of the composites when coupled to a lithium metal anode is found to be a function of the PEODT/MoS_2 ratio and clearly all the nanocomposites give a higher OCV value (2.62 V) than that observed (2.25 V) for pure MoS_2. The discharge capacity is also found to be significantly enhanced from 40 mAh g^{-1} for pristine MoS_2 to ~100 mAh g^{-1} for the nanocomposite. This can be attributed to the enhanced 'bidimensionality' and also to greater structural disorder in the composite [10,22]. In order to clarify the role of the polymer incorporation on the electrochemical performance on extended cycling, the variation in discharge capacities was measured for both MoS_2 and PEDOT/MoS_2 cathodes for several cycles, as shown in Fig. 5(b). For the PEDOT/MoS_2 composite, there is only a small loss in capacity over the first two cycles, and this demonstrates better coulombic efficiency for the discharge process. By contrast, for pristine MoS_2, the cell capacity drops substantially after five cycles Fig. 5(b). The reason for the poor cyclability in MoS_2 is thought to be the result of irreversible reactions of Li^+ ions with the lattice, and structural phase transformation [23] from the α-phase (2H-MoS_2) to the β-phase (disordered 1T-MoS_2) after the fifth cycle. This phase transition appears to be somewhat suppressed by the incorporation of PEDOT and explains why the PEDOT/MoS_2 nanocomposite maintains a capacity of over 90 mAh g^{-1} for several cycles.

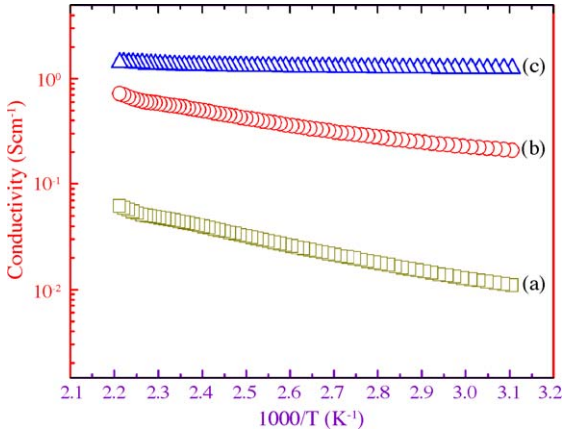

Fig. 4. Variation of electrical conductivity of (a) pristine MoS_2, (b) PEDOT/MoS_2 nanocomposite and (c) PEDOT with temperature measured using a four probe set-up.

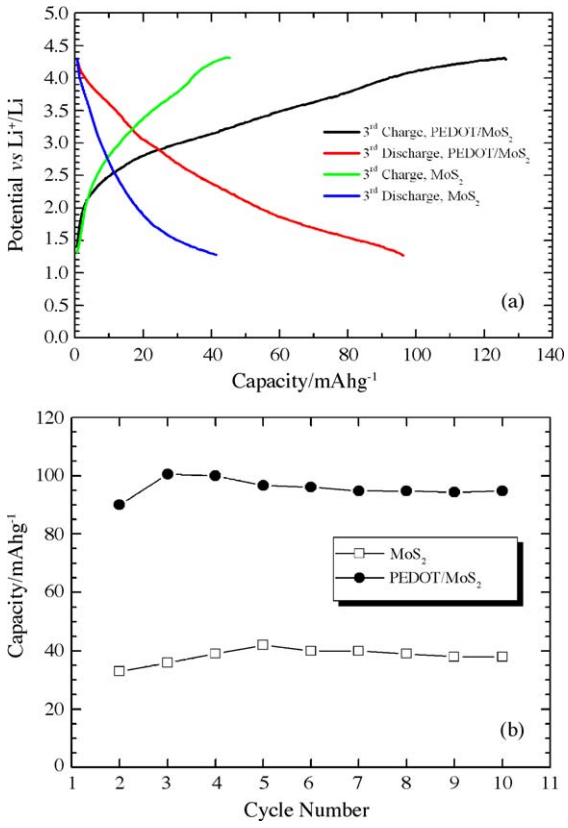

Fig. 5. (a) Potential vs. specific capacity for third cycle of pristine MoS_2, and PEDOT/MoS_2 nanocomposite. Potential range was selected to be 1.0–4.4 V vs. Li^+ after coupling with lithium metal anode and 1 M $LiClO_4$ in a mixed electrolyte of ethylene and dimethyl carbonate at room temperature using a constant current density of 15 mA cm^{-2}. (b) Evolution of discharge capacity with number of cycles for pristine MoS_2 and PEDOT/MoS_2. The data were obtained at a current density of 15 mA g^{-1}. The potential range was 2.0–4.4 V vs. Li^+/Li.

4. Conclusions

A method has been developed for interleaving poly(3,4-ethylenedioxythiphene) nanoribbons between the layers of MoS_2 using the soft chemistry route of intercalation. This reaction takes place with the in situ oxidative polymerization method in the presence of an external oxidizing agent. The addition of monomer and ferric chloride as oxidant to a suspension of single layers of MoS_2 cause flocculation during which the MoS_2 layers sandwich the PEDOT sheets in a remarkably well-ordered fashion to produce a single-phase product. Analysis of the experimental data presented here suggests that the polymerization proceeds concomitantly with intercalation. Our preliminary results also indicate that the discharge capacity is significantly enhanced from 40 mAh g^{-1} for pure MoS_2 to $\geq$100 mAh g^{-1} for the nanocomposite. The improved performance is presumably due to a higher electrical conductivity, and to the altered separation between the MoS_2 layers inducing molybdenum clustering which is related to some electron transfer from the guest species.

References

[1] M. Nath, A.K. Raychaudhuri, C.N.R. Rao, Chem. Phys. Lett. 368 (2003) 690.
[2] M. Nath, A. Choudhuri, A. Kundu, C.N.R. Rao, Adv. Mater. 15 (2003) 2098.
[3] U.K. Gautam, R. Seshadri, C.N.R. Rao, Chem. Phys. Lett. 375 (2003) 560.
[4] D.M. Kaschak, S.A. Johnson, D.E. Hooks, H.-N. Kim, M.D. Ward, T.E. Mallouk, J. Am. Chem. Soc. 120 (1998) 10887.
[5] Y.-S. Han, I. Park, J.-H. Choy, J. Mater. Chem. 11 (2001) 1277.
[6] A. Vadivel Murugan, B.B. Kale, C-W. Kwon, G. Campet, K. Vijayamohanan, J. Mater. Chem. 11 (2001) 2470.
[7] -G. Wu, D.C. DeGroot, H.O. Marcy, J.L. Schindler, C.R. Kannewurf, Y.-J. Liu, W. Hirpo, M.G. Kanatzidis, Chem. Mater. 8 (1996) 1992.
[8] T.A. Kerr, L.F. Nazar, Chem. Mater. 8 (1996) 2588.
[9] P. Gomez-Romero, Adv. Mater. 13 (2001) 163.
[10] A. Vadivel Murugan, C-W. Kwon, G. Campet, B.B. Kale, T. Maddanimath, K. Vijayamohanan, J. Power Sources 105 (2002) 1.
[11] K.E. Dungey, M.D. Curtis, J.E. Penner-Hahn, Chem. Mater. 10 (1998) 2152.
[12] L. Wang, J.L. Schindler, J.A. Tomas, C.R. Kannewurf, M.G. Kanatzidis, Chem. Mater. 7 (1995) 1753.
[13] T.L. Templeton, Y. Yoshida, X.-Z. Li, A.S. Arrott, A.E. Curzon, F. Hamed, M.A. Gee, P.J. Schurer, J.L. LaCombe, IEEE Trans. Magn. 29 (1993) 2625.
[14] G. Heywang, F. Jonas, Adv. Mater. 4 (1992) 116.
[15] H. Yamato, M. Ohwa, W. Wernet, J. Electroanal. Chem. 397 (1995) 163.
[16] A. Vadivel Murugan, C.W. Kwon, G. Campet, B.B. Kale, A.B. Mandale, S.R. Sainker, C.S. Gopinath, K. Vijayamohanan, J. Phys. Chem. B 108 (2004) 10736.
[17] I. Winter, C. Reese, J. Hormes, G. Heywang, F. Jonas, Chem. Phys. 194 (1995) 207.
[18] S. Ghosh, O. Inganas, Adv. Mater. 11 (1999) 1214.
[19] A.V. Powell, L. Kosidowski, A. McDowall, J. Mater. Chem. 11 (2001) 1086;
L. Kosidowski, A.V. Powell, Chem. Commun. (1998) 2201.
[20] L. Wang, J. Schindler, J.A. Thomas, C.R. Kannewurf, M.G. Kanatzidis, Chem. Mater. 7 (1995) 1753.
[21] C.D. Wagner, W.M. Riggs, L.E. Davis, J.F. Moulder, G.E. Muilenberg, Handbook of X-ray Photoelectron Spectroscopy, Perkin-Elmer Corporation, Eden Prairie, MN, 1979.
[22] N. Treuil, C. Labrugere, M. Menetrier, J. Portier, G. Campet, A. Deshayes, J.-C. Frison, S.-J. Hwang, S.-W. Song, J.-H. Choy, J. Phys. Chem. B 103 (1999) 2100.
[23] C. Julien, S.I. Saikh, G.A. Nazri, Mater. Sci. Eng. B 15 (1992) 73.